Estimation for Robotic Navigation

ARS4 Project Report

Ahmad SHOUR
Hasan KASSEM
Hussein LEZZAIK

Supervisor: Prof. Dr. BONNIFAIT Philippe

University of Technology of Compiègne
25th January 2021

Contents

List of Figures

List of Tables

1 Introduction

Determining the position of objects on the globe has been the subject of great interest since ancient times when people used stars to triangulate their positions. The advent of radar in the 1930s brought a major advance where the direction of targets could be measured by transmitting short radio pulses and measuring the direction of the strongest return[1].

In today's world, Unmanned Vehicles (UV's) are steadily finding applications in both civilian and military fields, specially in dull, dirty and dangerous mission scenarios, thus reducing potential risks to human life and increasing efficiency. Multiple UV applications are gaining precedence over single vehicle missions since they reduce the risk of failure and increases robustness while providing increased sensor coverage. These UV's can share their sensor information with the group to aid in objective completion. One such objective is vehicle localization. For a vehicle to be able for Cooperative Localization: Challenges and Future Directions to localize itself position information is necessary which is provided by the Global Positioning System (GPS). However, GPS signals may be jammed or spoofed and even though technology exists to overcome such obstacles. In such scenarios for a connected sensor network, vehicles cooperate to share their odometry and relative position information to collectively estimate the pose of all vehicles in the group [1].

The objective of this project is presented in section 2. Problem under study is presented in section 3, followed by mathematical modeling and experimental setup in section 4. We present our analysis and results in section 5, then we conclude and compare our results in section 6.

2 Objective

As mentioned briefly in Section 1, the problem of cooperative localization is used to facilitate navigation in GPS denied environments using the vehicle's motion information from it's internal sensors and the information about it's surroundings from it's external sensors. This exchange of information between the vehicles in the group in the presence of certain features whose position information is known a priori helps in generating vehicle state estimates for all vehicles in the group that enables completion of various tasks in GPS denied or jammed or spoofed environments or even in areas with high uncertainty in GPS signals like canyons, urban areas and so on.

The objective of this project is to study and evaluate on real experiments data fusion methods that improve the localization estimates of the two communicating vehicles that share information, one vehicle being equipped with a lidar.

3 Problem Description

The figure below shows two cooperative vehicles. The altitude z of the vehicles is assumed to be constant. The working frame R_O is East - North - Up (ENU), and R_M denotes the body frame associated with each vehicle, and is centered at the middle of the rear wheels.

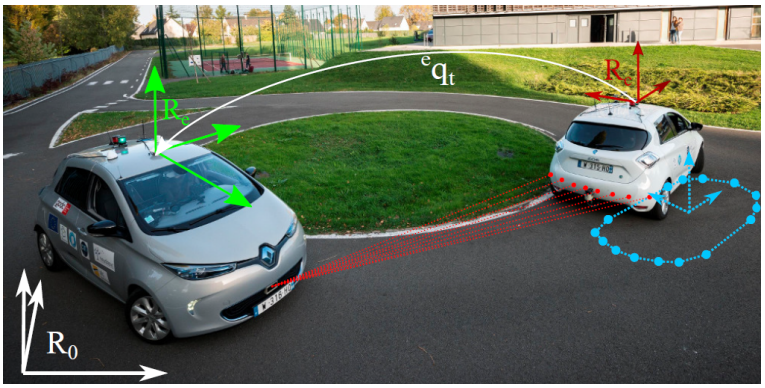

Figure 3.1.1: Two Zoe cars in the test track SEVILLE at UTC

We want to estimate the poses X of the two vehicles characterized by the Cartesian position x, y in the local ENU frame, and ψ the heading of each vehicle. The following section presents the available sensors and the data thus recorded during a test.

3.1 Available Sensors and the Dataset

The follower vehicle is equipped with the following:

1. A low cost L1-GNSS (GPS and GLONASS) receiver (ublox8T) which provides:
   - The position of the GPS antenna that is centered on point M of the vehicle body frame.
   - The position is computed by a Kalman filter integrated in the receiver (this is given in the dataset as "pos_gnss_f", "cov_gnss_f"). The track angle is also computed by the GNSS receiver. This track angle is equal the heading of the car as long as there is no slippage.
2. Dead-Reckoning (DR) sensors :
   - The vehicle speed measurement is obtained from the sensors of the rear wheels (Given in dataset as the first component of "vel_f").
   - A yaw rate gyro measuring the angular velocity is also available from the CAN bus (Given in dataset as the second component of "vel_f").
3. An Inertial Measurement Unit (IMU - SpanCPT) : with a very accurate dual-frequency GPS receiver that serves as ground truth (Given in the dataset as "pos_ref_f","cov_ref_f").
4. A front looking lidar SICK LD-MRS. The processing of the lidar impacts has been done by Elwan Héry. The center of the cluster corresponding to the leader has been computed in the

body frame of the follower (Given in the dataset as "pos_lidar_f","cov_lidar_f"). Translations have been compensated such that this estimate corresponds to the pose of the body frame of the leader (at point M) in the body frame of the follower (Figure 3.1.2).

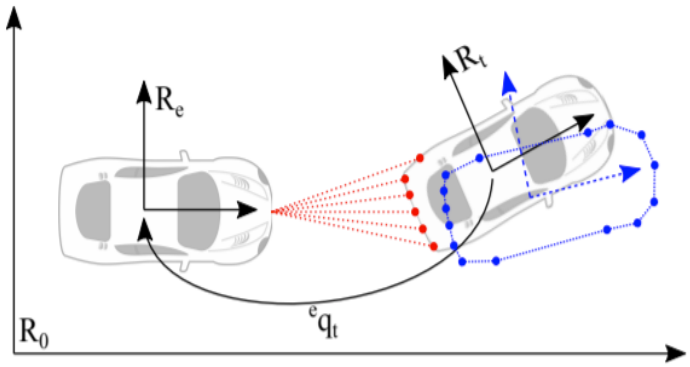

Figure 3.1.2: Lidar impacts and clustering and relative pose estimation

The dataset has been recorded by Elwan Héry, Stéphane Bonnet and Anthony Welte in July 2018 at UTC. A very accurate map of the evolution area is also provided for visualization only (Figure 3.1.3).

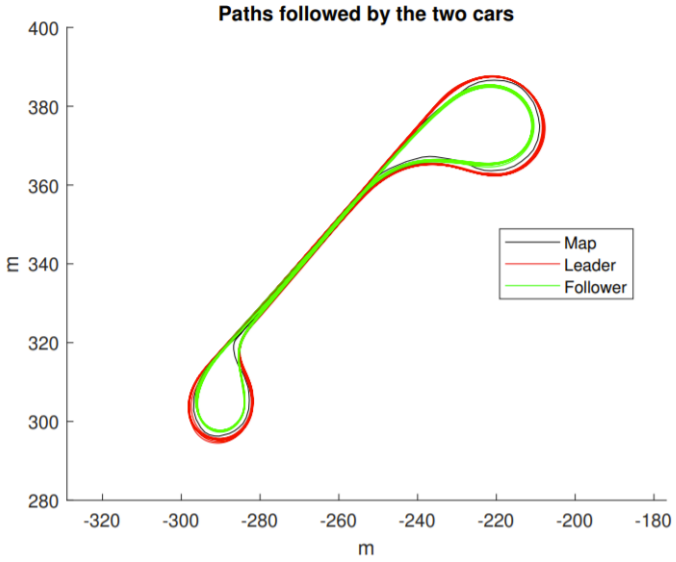

Figure 3.1.3: Paths followed by the two cars on SEVILLE. It can be noticed that their are quite different such that the follower can always see the leader in its lidar field of view.

In the experiment, the information transmitted by the communication modems has not been logged. The data of both vehicles have been logged by two separated computers with

timestamps in the same reference time, thanks to an accurate GPS time synchronization mechanism. Moreover, even if the raw measurements are asynchronous, they have been re-synchronized at the frequency of the lidar for simplification the sampling time is around 0.08s.

3.2 Addressed Scenarios

We will study and analyze data fusion methods in multiple experimental settings and filter features, and then conclude with a comparison between them all. The following scenarios will be studied during this report:

- Vehicles are not communicating and the Lidar is not used. subsection 5.1
- The leader is sending its position to the follower, while the latter uses its Lidar. A Taylor Series approximation approach will be used to handle uncertainty propagation. subsection 5.2
- The same scenario as the previous one, except that an unscented transform approach will be used to handle uncertainty propagation . subsection 5.3
- The leader is sending its position to the follower, while the latter uses its Lidar. And the follower also sends its global position along with the Lidar measurement to the leader. The Kalman update stage will then be replaced by a covariance intersection update. subsection 5.4

4 Analysis Setup

4.1 System Modeling

The following state space representation will be used for both the leader and the follower. Our state vector can be represented as follows:

$$X = \begin{pmatrix} x \\ y \\ \psi \\ v \\ \omega \\ T \end{pmatrix} \tag{1}$$

Where (x, y, ψ) represents the pose of the vehicle, v represents the speed in the direction of motion, w represents the angular velocity, and T represents the sampling period between two consecutive measurements.

Both the linear and angular velocities, and the sampling period, are assumed to be constant in the evolution model, and are only affected by white noise. Using simple kinematic model of a vehicle, the following equations will represent the discrete-time evolution of the system:

$$\begin{pmatrix} x_{k+1} \\ y_{k+1} \\ \psi_{k+1} \\ v_{k+1} \\ \omega_{k+1} \\ T_{k+1} \end{pmatrix} = \begin{pmatrix} x_k + T_k v_k \cos(\psi_k) \\ y_k + T_k v_k \sin(\psi_k) \\ \psi_k + T_k w_k \\ v_k \\ \omega_k \\ T_k \end{pmatrix} + \alpha_k \tag{2}$$

Where α_k is a white noise with covariance matrix Q. The Kalman prediction stage will be governed by (2) and its Jacobian with respect to X_k, given by:

$$J_k = \frac{\partial X_{k+1}}{\partial X_k} = \begin{pmatrix} 1 & 0 & -T_k v_k \sin(\psi_k) & T_k \cos(\psi_k) & 0 & v_k \cos(\psi_k) \\ 0 & 1 & T_k v_k \cos(\psi_k) & T_k \sin(\psi_k) & 0 & v_k \sin(\psi_k) \\ 0 & 0 & 1 & 0 & T_k & w_k \\ 0 & 0 & 0 & 1 & 0 & 0 \\ 0 & 0 & 0 & 0 & 1 & 0 \\ 0 & 0 & 0 & 0 & 0 & 1 \end{pmatrix} \tag{3}$$

This evolution model will be used in all studied problem variations. The observers will be designed specific to each addressed problem in its associated section.

4.2 Noise

4.2.1 Measurement Noise

System observers noise are considered white, with covariance matrices R_k determined using the dataset given; using the covariance matrices of each measurement.

The standard deviation of measuring T will be taken 0.002^2 (setting this value to zero didn't change the results), and measurements of different sensors are assumed to be uncorrelated.

4.2.2 Filter Tuning: Process Noise

The matrix Q defined in the previous section will be used to tune our filters. First, we assumed that Q_{11}, Q_{22}, and Q_{33} are zero (which represent no process noise for (x, y, ψ)). Using these values, the filters showed high inconsistencies, which can be justified by the fact that the evolution equations don't model exactly the system (zero acceleration assumption).
As expected, there was a trade-off between consistency and accuracy. Increasing the variances in Q resulted in more consistent but less accurate results. However, the accuracy change was found to be negligible (in the order of millimeters), while consistency can change dramatically.
Different values were tested. The Used values of Q_{11}, Q_{22}, Q_{33} will be specified when presenting the results, and the variances of the other state variables were set to those of their corresponding measurements (Changing these values didn't reflect significant change in performance).

4.3 Filter Evaluation

For each experiment, results were evaluated in terms of consistency and accuracy. Having a ground truth in our dataset, accuracy was measured by how far is the mean of the filter's estimations from the mean of the ground truth values, of each of the states (x, y, ψ). The maximum absolute value of the errors is also reported.
Consistency is measured as the percentage of the estimation errors that falls within $\pm 3\sigma$, where σ is the standard deviation of the state variable under study.

5 Analysis and Results

Having defined our system model and its parameters, we will now address each experiment, define the observation model, and present the results.

5.1 Scenario 1: Loosely Coupled System

The goal here is to improve the localization of each vehicle by doing the data fusion of its Ublox with its DR sensors in a loosely coupled way. The localization of each vehicle will be performed independently and without communication between the vehicles.

5.1.1 Observers Design

For each vehicle, the observers design will be the same.
Given our dataset, the following equation will represent the measurement design of our system:

$$Y_k = CX_k + \beta_k$$

where:

- Y_k is the observation vector, built from the dataset (pos_gnss_f for $(x_{gps}, y_{gps}, \psi_{gps})$, vel_f for (v_{od}, ω_{od}), and time differences for T_{meas}):

$$Y_k = \begin{pmatrix} x_{gps} \\ y_{gps} \\ \psi_{gps} \\ v_{od} \\ \omega_{od} \\ T_{meas} \end{pmatrix}$$

- X_k is the state vector.
- $C = I_6$ is the identity matrix.
- β_k is a white noise with covariance matrix R_k.

5.1.2 Results

After proper tuning, the values of Q_{11}, Q_{22}, Q_{33} for both vehicles is set to 0.3. The following plot was generated, representing the estimation errors and the bounds of the $\pm 3\sigma$.

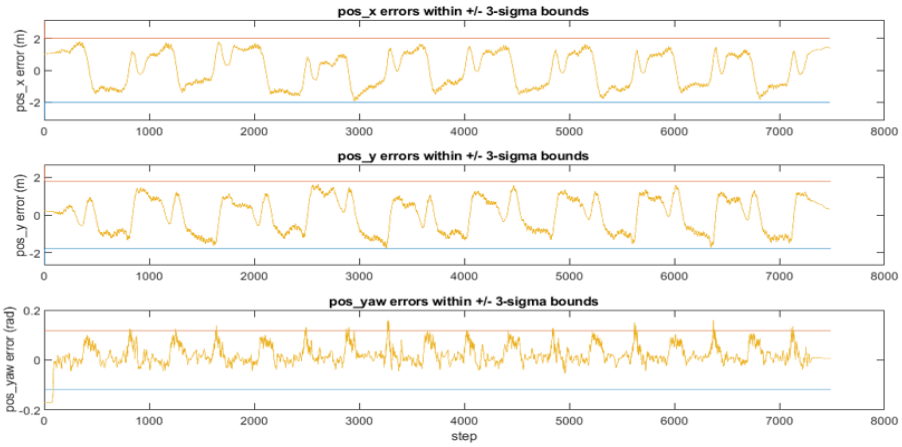

Figure 5.1.4: Follower Pose errors within $\pm 3\sigma$ bounds.

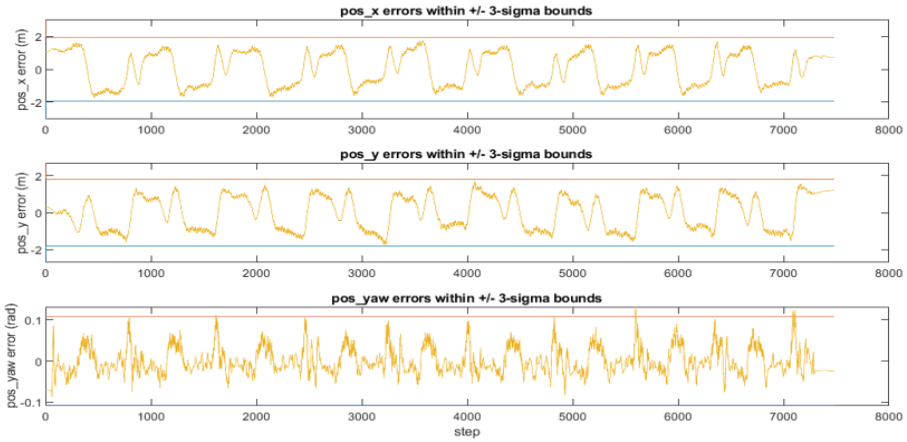

Figure 5.1.5: Leader Pose errors within $\pm 3\sigma$ bounds.

The following table presents the mean, max, and consistency of errors of each vehicle:

	Follower			Leader		
	x	y	ψ	x	y	ψ
Mean Error	0.0597	-0.0010	0.0197	0.0235	0.0066	-0.0001
Max abs. Error	1.9488	1.7488	0.1698	1.7797	1.7300	0.1313
% outide $\pm 3\sigma$	100	100	98.2498	100	100	99.8263

Table 5.1.1: Numerical Results of 1st Scenario (SI Units)

5.2 Scenario 2: The Follower Knows The Leader's Position

The goal is to improve the localization of the follower by doing the data fusion of its DR sensors with its own Ublox and the received pose of the leader translated into its own body frame, thanks to the estimated relative pose obtained from the lidar measurements.
In this problem, we consider the following additions:

- The leader sends its estimated pose with the associated covariance matrix.
- The follower can now benefit from the measurements of its Lidar by fusing them with the leader's received pose.

5.2.1 Frames Transformation and Uncertainty Propagation

We will introduce two operators for frame transformation that also handle for uncertainty. The work is taken from [2].

Let ${}^{j}q_i = ({}^{j}x_i, {}^{j}y_i, {}^{j}\psi_i)^T$ denote the pose of the frame R_i in the frame R_j, with uncertainty represented by the covariance matrix $P_{{}^{j}q_i}$. The compound operator $\oplus$ is defined as:

$$ {}^{k}q_i = {}^{k}q_j \oplus {}^{j}q_i = \begin{pmatrix} \cos({}^{k}\theta_j) & -\sin({}^{k}\theta_j) & 0 \\ \cos({}^{k}\theta_j) & \cos({}^{k}\theta_j) & 0 \\ 0 & 0 & 1 \end{pmatrix} \tag{4} $$

$$ P_{{}^{k}q_i} \approx J_{\oplus} \begin{pmatrix} P_{{}^{k}q_j} & P_{{}^{k}q_j, {}^{j}q_i} \\ P_{{}^{j}q_i, {}^{k}q_j} & P_{{}^{j}q_i} \end{pmatrix} J_{\oplus}^{T} $$

$\oplus$ combines the global pose of R_j in R_k, and the relative pose of R_i in R_j, to give a global pose of R_i in R_k.
The operator $\ominus$ inverts the pose-frame representation, given by:

$$ {}^{i}q_j = \ominus {}^{j}q_i \tag{5} $$

$$ P_{{}^{i}q_j} \approx J_{\ominus} P_{jqi} J_{\ominus}^{T} $$

$$ \text{where } J_{\ominus} = \begin{pmatrix} -\cos({}^{j}\theta_i) & -\sin({}^{j}\theta_i) & {}^{j}x_i \sin({}^{j}\theta_i) - {}^{j}y_i \cos({}^{j}\theta_i) \\ \sin({}^{j}\theta_i) & -\cos({}^{j}\theta_i) & {}^{j}x_i \cos({}^{j}\theta_i) + {}^{j}y_i \sin({}^{j}\theta_i) \\ 0 & 0 & -1 \end{pmatrix} = \begin{pmatrix} -\cos({}^{j}\theta_i) & -\sin({}^{j}\theta_i) & {}^{i}y_j \\ \sin({}^{j}\theta_i) & -\cos({}^{j}\theta_i) & -{}^{i}x_j \\ 0 & 0 & -1 \end{pmatrix} $$

Note that the propagated uncertainty is calculated based on a Taylor series approximation, which will be modified in the next section.
These two operators will be used to combine the leader's global position received by the follower, and the leader's relative position from the Lidar, to give a global position measurement of the follower.

5.2.2 Observers Design

The observers from section 5.1.1 will be used for each vehicle, with an addition of a new observer system for the follower only.

Let the measures pose from the Lidar be ${}^{f}q_l$ and the leader pose received by the follower be ${}^{G}q_l$. These measurements give the following observation model:

$$Y_{k,lidar} = C_{lidar} X_k + \gamma_k$$

where:

- $Y_{k,lidar}$ is the observation vector, given by:

$$Y_{k,lidar} = {}^{G}q_f = {}^{G}q_l \oplus (\ominus {}^{f}q_l)$$

- X_k is the state vector.
- $C = I_3$ is the identity matrix.
- γ_k is a white noise with covariance matrix given by the transformations defined previously, $P_{{}^{G}q_f}$.

Kalman update phase will consider the above observation equation whenever a usable Lidar measurement is available. The dataset given has a flag ***usable*** that tells if the current Lidar measurement can be used.
However, the usable Lidar measurements also contained outliers, for which we implemented a Mahalanobis test to reject them. The following figure shows the Mahalanobis distances calculated during the test:

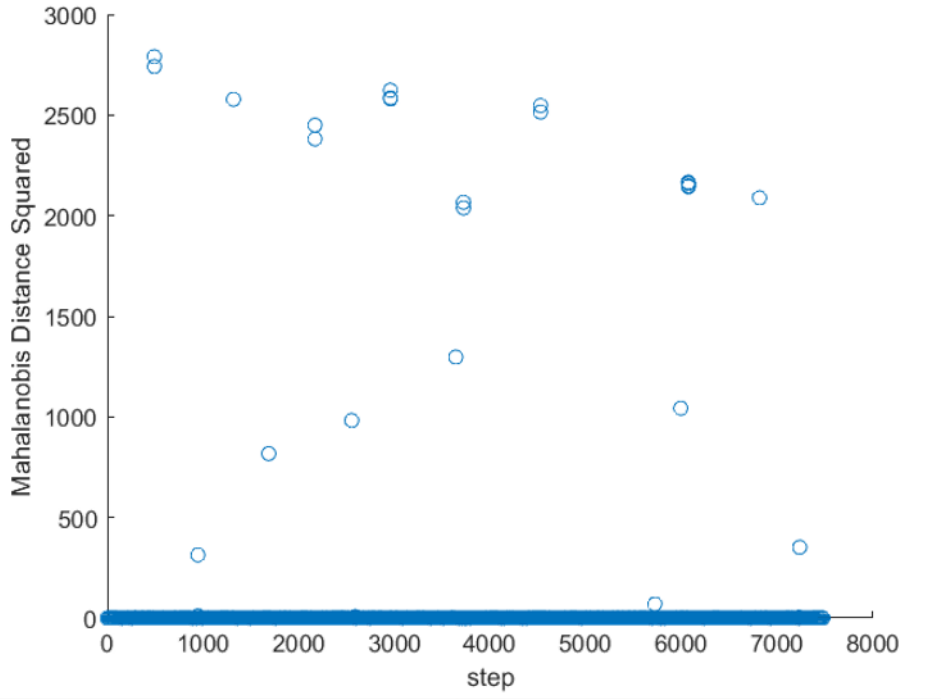

Figure 5.2.6: Squared Mahalanobis distance calculations showing presence of outliers.

5.2.3 Results

After proper tuning, the first three diagonal terms of Q of the follower were set to 0.8. The leader, of course, has no change in results. The following plot was generated, representing the estimation errors and the bounds of the $\pm 3\sigma$.

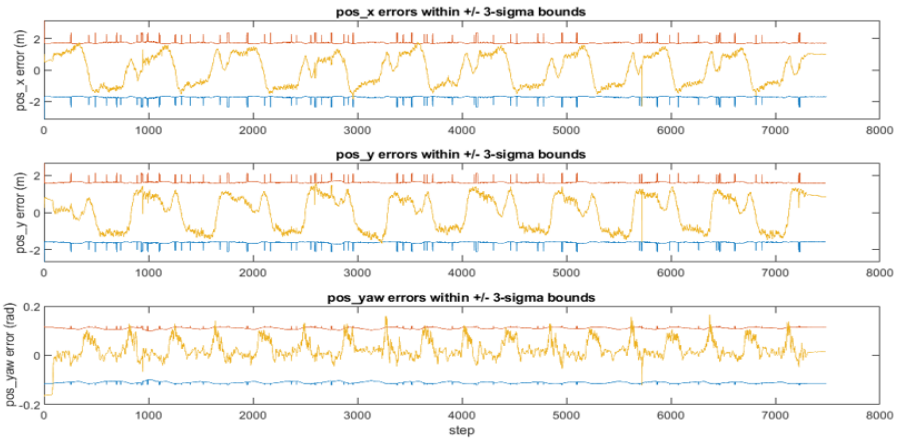

Figure 5.2.7: Follower Pose errors within $\pm 3\sigma$ bounds.

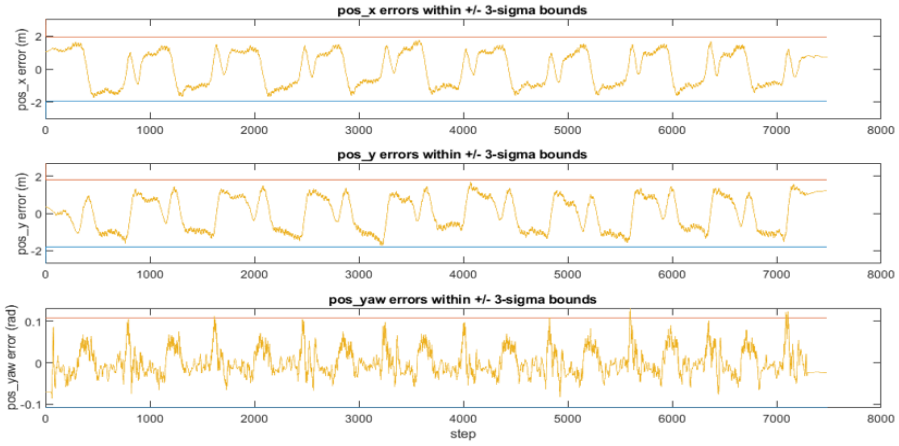

Figure 5.2.8: Leader Pose errors within $\pm 3\sigma$ bounds.

The following table presents the mean, max, and consistency of errors of each vehicle:

	Follower			Leader		
	x	y	ψ	x	y	ψ
Mean Error	0.0548	0.0219	0.0226	0.0235	0.0066	-0.0001
Max abs. Error	2.3491	1.6678	0.1699	1.7756	1.7256	0.1313
% outide $\pm 3\sigma$	99.7597	99.8798	97.3146	100	100	99.8263

Table 5.2.2: Numerical Results of 2nd Scenario (SI Units)

5.3 Scenario 3: Introducing the Unscented Transform

This scenario is the same as the previous one, but more consistent $\oplus$ and $\ominus$ functions are going to be used by the Unscented Transformation (UT).

5.3.1 The Unscented Transform

The unscented transform addresses the general problem of approximating a non-linear transformation of a random variable. We will present briefly how to apply UT, more details can be found in [2].
Consider a random variable x with known mean m_x and convariance matrix P_x. Let $y = T(x)$ be a non-linear transformation of x. Then, the mean and covariance of y can be approximated by:

$$m_y = \sum_{n=1}^{N} \omega^i y^i$$

$$P_y = \sum_{n=1}^{N} \omega^i (y^i - m_y)(y^i - m_y)^T$$

where $y^i = T(x^i)$, x^i are samples taken from the distribution of x, and w^i are their associated weights. Several sampling methods can be used. Our samples are defined by the sample m_x with weight w_0 and the following set:

$$\{m_x \pm \sqrt{\frac{n}{1-w_0}}\sqrt{D_i}V_i | i = 1, 2, \dots n\}$$

where D_i are the eigen values of P_x, V_i are the corresponding eigen vectors, n is the dimension of x, and all these samples are equally weighted with $w = \frac{1-w_0)}{2n}$.

5.3.2 Frame Transformation with UT

For $\ominus$ operator, one can represent (5) as a non-linear transformation ${}^iq_j = T({}^jq_i)$, from which, therefore, the procedure presented in the previous subsection can be carried out straightforward.
For the $\oplus$ operator, we consider a random variable defined by the concatenation of ${}^kq_j$ and ${}^jq_i$ into a 6-dimensional vector $\tilde{q} = ({}^kq_j, {}^jq_i)^T$. Hence, (4) can be represented as a non linear transformation ${}^kq_j = T(\tilde{q})$, and then the procedure of UT can be carried out directly.

5.3.3 Results

After proper tuning, the same parameters of the Q matrix from the previous section were used. In addition, the tuning parameter w_0 for sampling the sigma points of the unscented transform for the $\oplus$ operator was found to be 0.95 as the best, and that for the $\ominus$ operator is found to be $1/7$. The following plot was generated, representing the estimation errors and the bounds of the $\pm 3\sigma$.

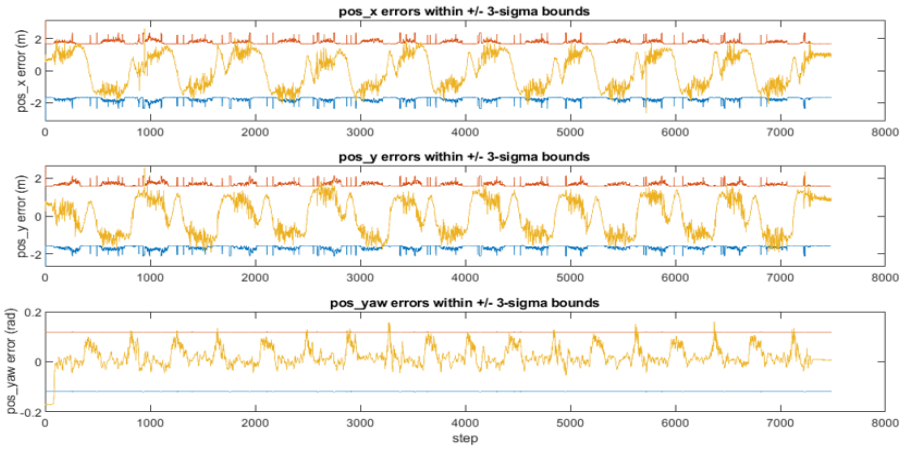

Figure 5.3.9: Follower Pose errors within $\pm 3\sigma$ bounds.

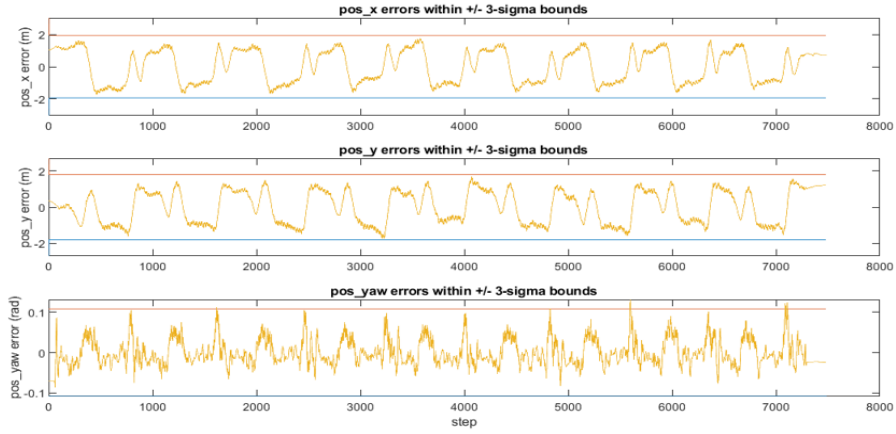

Figure 5.3.10: Leader Pose errors within $\pm 3\sigma$ bounds.

The following table presents the mean, max, and consistency of errors of each vehicle:

	Follower			Leader		
	x	y	ψ	x	y	ψ
Mean Error	0.0122	0.0153	0.0197	0.0235	0.0066	-0.0001
Max abs. Error	2.6826	2.5207	0.1700	1.7756	1.7256	0.1313
% outide $\pm 3\sigma$	99.3854	99.6927	98.2632	100	100	99.8263

Table 5.3.3: Numerical Results of 3rd Scenario (SI Units)

5.4 Scenario 4: Both Vehicles Exchange Data

The goal is to improve the localization of the two vehicles by doing the data fusion of all the sensors. In other words, each vehicle has to merge its DR sensors with its own Ublox and to use the pose received from the other. The follower has to solve the same problem as before, but the leader has now to exploit the received relative pose and the received estimated pose of the follower.
In this problem, we use the Covariance Intersection (instead of a Kalman update) [3] because there is now a cycle in the information exchange.

5.4.1 Update Phase

For each vehicle, the update due to the measurements of each one's own GNSS and DR observation will be carried out as before with Kalman update. However, there is an addition observation for each vehicle now:

- For the follower, it has the same new measurement as stated in the previous two sections.
- For the leader, the new observation for the state variables (x, y, ψ) is given by: $Y_{obs} = {}^{G}q_f \oplus {}^{f}q_l$, where ${}^{G}q_f$ is global pose of the follower reveived by the leader, and ${}^{f}q_l$ is the Lidar measurement sent by the follower.

To perform the update step of these new measurements, Covariance Intersection [2] will be used. For either vehicle, let x_1 be its current pose, and let x_2 be the observation of the pose calculated from the data received from the other vehicle. P_i denote the covariance matrix associated to x_i, $i = 1, 2$. Then, Covariance intersection update is governed by the following equations, giving the updated state variable $\hat{x}$ with its updated covariance P:

$$P^{-1} = \omega P_1^{-1} + (1 - \omega) C^T P_2^{-1} C$$

$$\hat{x} = x_1 + (1 - \omega) P C^T P_2^{-1} (x_2 - C x_1)$$

where C is the observation design matrix (Identity matrix in our application), and ω is the optimal value in $[0, 1]$ minimizing the determinant of P.

5.4.2 Results

After tuning, we found that using the optimal ω for covariance intersection update gives bad accuracy (worse than loosely coupled system). Despite of tuning many parameters (ω for CI, Q entries, outlier rejection thresholds...), the results kept alternating between either bad accuracy or highly ***nervous*** errors. The following plot show the results of using $\omega = 0.1, Q$ values were set to be 0.5, and Lidar data outlier rejection thresholds of 20 for both vehicles:

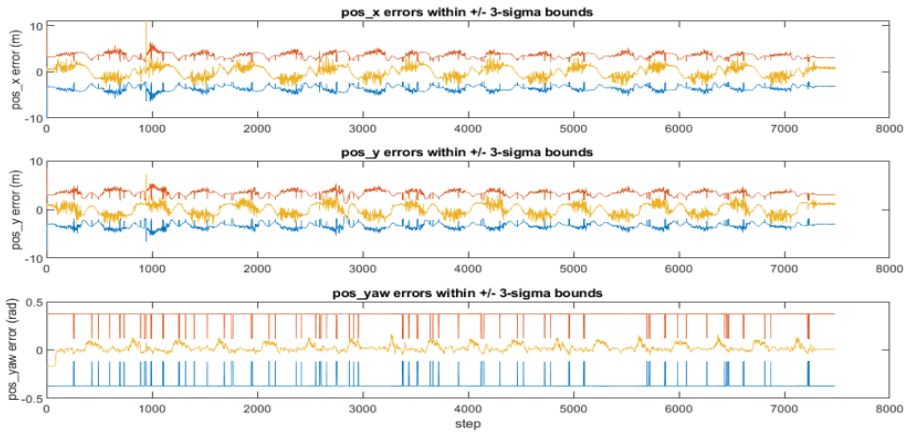

Figure 5.4.11: Follower Pose errors within $\pm 3\sigma$ bounds.

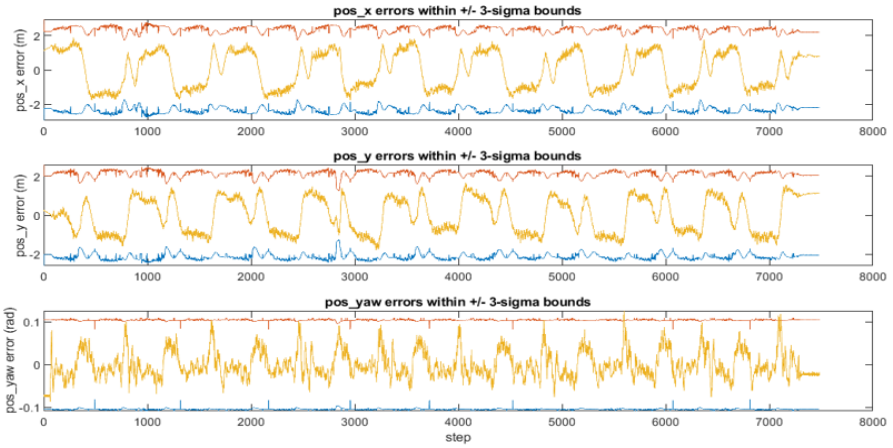

Figure 5.4.12: Leader Pose errors within $\pm 3\sigma$ bounds.

The following table presents the mean, max, and consistency of errors of each vehicle:

	Follower			Leader		
	x	y	ψ	x	y	ψ
Mean Error	-0.0054	0.0061	0.0203	0.0104	-0.0107	-0.0001
Max abs. Error	11.1149	7.1336	0.1709	1.8889	1.7975	0.1260
% outide $\pm 3\sigma$	99.9866	99.7194	100	100	100	99.8130

Table 5.4.4: Numerical Results of 4th Scenario (SI Units)

6 Conclusion

Comparsion between Filters

Comparing scenario 1 with the other ones, an obvious result can be deduced that cooperation will most likely improve the performance of localization. After exchanging information, both accuracy and consistency were improved moving from scenario 1 to 3. Using Lidar data without unscented transform, however, showed similar results to the loosely coupled system. But when frame transformation was applied through unscented transform, accuracy was greatly improved. (from about 5cm in x into about 1cm).

Now regarding the last scenario, despite that it showed very high accuracy with excellent consistency, the results also showed high maximum errors for the follower, and highly ***nervous*** plot of the system errors. The system may therefore need further tuning or more robust assumptions for merging the data exchanged...

References

[1] Gao, C.; Zhao, G.; Fourati, H. Cooperative Localization and Navigation: Theory, Research, and Practice; CRC Press:Boca Raton, FL, USA, 2019.

[2] Multi-Sensor Fusion and Estimation for Robotic Navigation, by Dr. BONNIFAIT Philippe 2020

[3] Probabilistic Robotics, by Dieter Fox, Sebastian Thrun, and Wolfram Burgard (2nd edition)